# 1.- Introduction

An important characteristic of the troposphere over the west coast of South America is the extreme dryness along the Atacama Desert. A strong and highly permanent subtropical anticyclone and the cold oceanic Humboldt Current are the main factors for this aridity. During early hours, dense stratocumuli ("camanchacas") are usually covering the coastal desert. An annual cycle, El Niño Southern Oscillation (ENSO), and a drastic change during the mid 70's are variabilities observed during the years in northern Chile [17] [18].

The NCEP/NCAR Reanalysis project reanalyses historical atmospheric data from 1948 to the present using state-of-the-art models. The data is obtained from many international sources. Spectral Statistic Interpolation and the Global Spectral Model are used for data assimilation. Finally, the output NCEP/NCAR Reanalysis data files of the atmospheric variables are in a 17 vertical pressure level on a 2.5º x 2.5º global grid every 6 hours.

The objective of this work is to study a 52-year monthly average series of Pressure, Temperature, Specific Humidity, and Precipitable Water Vapour (PWV) using the NCEP/NCAR Reanalysis data at the closest grid point (25.0º S, 70.0º W) to Paranal, at the surface and at 850, 500, and 300 mb.

Section 2 describes the NCEP/NCAR Reanalysis project and its three major modules (data decoder and quality control preprocessor, data assimilation, and reanalysis output module). A discussion of the reliability of the reanalysis data and a description of previous studies in Visviri and Chajnantor are included. Section 3 describes the climatology of the Atacama Desert and shows the estimations used for the Paranal area. Section 4 shows the methodology used for this work, explaining how the data is obtained and how is displayed using GrADS and Matlab. Section 5 shows the analysis of the data, where the atmospheric variables Pressure, Temperature, Precipitable Water Vapour, and Specific Humidity are displayed for the period from 1948 to September 2000, at the surface and at 850, 500, and 300 mb. The analysis focuses in seasonal and interannual cycles rather than daily cycles. Section 6 concludes from the analysis obtained from the NCEP/NCAR Reanalysis data and gives some suggestions for future works.

# 2.- Overview of the Reanalysis System

## 2.1.- Reanalysis system

The NCEP/NCAR Reanalysis project is a joint project between the National Center for Environmental Prediction (NCEP, formerly "NMC") and the National Center for Atmospheric Research (NCAR). The goal of this joint effort is to produce new atmospheric analyses using historical data (1948 onwards) and also to produce analyses of the current atmospheric state (Climate Data Assimilation System, CDAS). This effort involves the recovery of land surface, ship, rawinsonde (**ra**diosonde and **win**d observations), pibal (**pi**lot **bal**loon observations), aircraft, satellite, and other data.

The basic idea of the reanalysis project is to use a frozen state-of-the-art analysis/forecast system and perform data assimilation using past data from 1948 to the present (reanalysis). The SSI analysis and the T62 Global Spectral Model are two of the three principle components (the third being the observation quality control programs) of the data assimilation module. A 6-hour forecast is performed to do **analysis**. The Spectral Statistics Interpolation (SSI) corrects the time integration toward the observed values. Then, the **reanalysis** is done at NCEP using T62 Global Spectral Model of 28 vertical levels. The system cycles on itself. The T62 Global Spectral Model moves the system along in time, the SSI corrects the time integration toward the observed values, providing the initial conditions for the next 6-hour integration. The output reanalysis files of atmospheric variables are on a 2.5º x 2.5º global grid of 17 vertical levels every 6 hours.

The same frozen analysis/forecast system will continue to perform data assimilation into the future so that climate researchers can asses whether current climate anomalies are significant when compared to a long reanalysis without changes in the data assimilation system

The next three sections (2.2, 2.3, and 2.4) are mainly based on the work made by Kalnay et al [1]. The NCEP/NCAR reanalysis system has three major modules: Data decoder and quality control preprocessor, Data assimilation module, and Reanalysis output module.

## 2.2.- Data decoder and quality control preprocessor

This is a major task performed at NCAR. Surface and upper-air observations are prepared for reanalysis reformatting the data coming from many different sources into a uniform BUFR (Binary Universal Format Representation).

### 2.2.1.- Data collection

The data is obtained world-wide from many international sources such as Global Telecommunication System (GTS), NOAA/National Environmental Satellite Data and Information System (NESDIS), Geophysical Fluid Dynamics Laboratory (GFDL), United Kingdom Meteorological Office (UKMO), Japanese Meteorological Agency (JMA), European Center for Medium-Range Weather Forecasts (ECMWF), among others.

The collected datasets are:

- Global rawinsonde data
- COADS (Comprehensive Ocean-Atmosphere Data Set) surface marine data
- Aircraft data
- Surface land synoptic data
- Satellite sounder data
- SSM/I (Special Sensing Microwave/Imager) surface wind speeds
- Satellite cloud drift winds.

Most of this information covers the period from about 1948 to the present, with some data not available for different periods. For example, the rawinsonde observing networks for Antarctica and the West Coast of South America did not start until July 1957, new satellite data is becoming available throughout the years, SSM/I became available in July 1987, etc.

On the question on how to handle the inevitable changes in the observation system, (specially new satellite data) the use of all the available data at a given time was chosen instead of selecting a subset of the observations that remain stable throughout the period of reanalysis. This lead to an analysis that is as accurate as possible throughout the 52-years reanalysis.

### 2.2.2.- Data preprocessor

The purpose of the preprocessing reanalysis module is to reformat the data coming from many different sources into a uniform BUFR format.

The preprocessor also detects major data problems, such as wrong dates, wrong locations, satellite data with wrong longitudes, garbled information, etc. The preprocessor includes preparation of the surface boundary conditions

- Satellite data: A special "satellite TOVS (TIROS-N Operational Vertical Sounder) soundings data monitoring system" has been developed to quality control of the data in the NESDIS archives tapes that can suffer from errors in dates and orbits. Satellite data in grid boxes of 10º x 10º, as well as single satellite observations, are quality controlled.

- Complex Quality Control with temporal check: The CQC system (described in 2.3) is included in the preprocessor but without the use of the first-guess of the model. It allows for the detection of changes in the station locations.

- Climatological Quality Control (QC) test of data: It checks expressing an observation anomaly in units of standard deviation with respect to climatology statistics. Such a check allows human monitors to check for unusual data present in unusual amounts, before the execution of the monthly reanalysis, and provides Optimal Interpolation Quality Control (OIQC) with additional information that can be used by its Decision Making Algorithm (DMA) as input to reanalysis.

- Boundary fields: The following analyses and climatologies are used:

- Sea Surface Temperature (SST): The United Kingdom Meteorological Office (UKMO) Global Ice and Sea Surface Temperature dataset (GISST) is used before 1982 and Reynolds reanalysis for 1982 on, when Advanced Very High Resolution Radiometer (AVHRR) data became available.
- Snow cover: The model uses NESDIS (NOAA/National Environmental Satellite Data and Information System) weekly analyses and climatology, updated weekly.
- Sea ice: Ice fields derived from Joint Ice Center analyses when available (before 1979), Scanning Multichannel Microwave Radiometer/Special Sounding Microwave Imager (SMMR/SSMI) (1979-1993), and Grumbine algorithm (beyond 1993) are being used. These have been incorporated into the SST analysis so that all values below –1.8ºC are considered sea ice.
- Albedo: The work done by Matthews (1995) is used [2].
- Soil wetness: The model uses [3] and [4] soil model.
- Roughness length: It is obtained from Simple Biosphere Model (SiB) [5].
- Vegetation resistance: Same as roughness length, from SiB.

## 2.3.- Data assimilation module

The central module is the data assimilation, which has the following characteristics:

- Analysis Scheme: Spectral Statistical Interpolation (SSI), a three-dimensional variational analysis scheme is used as the analysis module [6] [7]; An important advantage of the SSI is that the balance imposed on the analysis is valid throughout the globe, thus making unnecessary the use of nonlinear normal-mode inizialitation. Improvements in error statistics and the use of the full tendency of the divergence equation in the cost function are included.

- Model: The T62/28-level (Triangular 62-waves truncation) NCEP Global Spectral Model is used with 28 vertical levels and a 210 km horizontal resolution. The model includes parameterizations of all major physical processes, like convection, large-scale precipitation, shallow convection, gravity wave drag, radiation with diurnal cycle and interaction with clouds, boundary layer physics, an interactive surface hydrology, and vertical and horizontal processes. Details of the model are described in [8] and [9].

- Complex Quality Control of rawinsonde data: The method of complex quality control CQC is used to quality control rawinsonde heights, temperatures and the mandatory and significant level rawinsonde winds [10].

- Optimal Interpolation Quality Control of all data: OIQC detects and withhold the data containing gross errors generated by instrumental, human, or communication-related mistakes that may occur during the process of making or transmitting observations [11] [12].

- BUFR observation "event" files: The final step in observation preprocessing (section 2.2.2) consolidates incoming data from all sources into BUFR files. Provisions have been made to archive in the reanalysis BUFR files, along with each original observation, a spectrum of processing information, collectively known as "events". These indicate the observation's source, all quality control decisions and their sources, a history of all modifications made to the observation prior to the analysis, and various background quantities relevant to the analysis process (i.e. interpolated first-guess values, interpolated analyzed values, interpolated climatological values and variances, and observation errors estimates).

- Optimal Averaging (OA) [13]: NCEP/NCAR Reanalysis includes not only the computation of grid point values but also temporal and spatial averages over some prescribed areas. This OA method increases the ability for detection of climate change.

- Periodic forecasts from the reanalysis: 8-day forecast every 5 days are performed, useful for predictability studies, indirect estimates of the accuracy of the analysis, and estimates of the impact of changes in the observing systems.

## 2.4.- Reanalysis output module

The reanalysis gridded fields have been classified into four classes, depending on the relative influence of the observational data and the model on the gridded variable. An A-class indicates that the analysis variable is strongly influenced by observational data, and hence it is the most reliable class. B-class indicates that, although there are observational data that directly affect the value of the variable, the model also has a very strong influence on the analysis value. C-class indicates that there are no observations directly affecting the variable, so that it is derived solely from the model fields forced by the data assimilation to remain close to the atmosphere. D-class represents a field that is obtained from climatological values and does not depend on the model. A list of output variables in GRIB format classified by class and pressure levels is included (appendix 1).

The reanalysis output module includes several different archives:

- BUFR observational archive: Reanalysis observational data undergo multiple processing stages in BUFR format.

- Main synoptic archive: Contains a large number of analysis and first-guess "pressure" fields at 00:00, 06:00, 12:00, and 18:00 UTC on a 2.5º latitude x 2.5º longitude grid. It also contains the "flux", "diagnostic", and "sigma" files used on the model Gaussian grid 192 x 94 points, and restart files at full resolution.

- Reduced "time series" Archive: This archive contains basic upper-air parameters on standard pressure levels saved in GRIB and NetCDF format readable with GrADS (Grid Analysis and Display System) software. The 17 pressure levels used are 1000, 925, 850, 700, 600, 500, 400, 300, 250, 200, 150, 100, 70, 50, 30, 20, and 10 mb. Data fields are saved on a 2.5º lat x 2.5º long grid (144 x 73). It contains data from 1948 onwards, 4x daily at 00:00, 06:00, 12:00, and 18:00 UTC, daily and monthly averages and long-term mean.

- Quick-look CD-ROM: Database that fit in a small (1 per year) number of CD-ROMs.

- Automatic monitoring system for the reanalysis output: At the end of each month of reanalysis, time series at all standard pressure levels are checked with a preliminary climatology based on NCEP's GDAS. Monthly averages, standard deviations of monthly mean, of the tendency, and of the interpolation check are computed.

The files used for this study are the Reduced "time series" Archive provided by the NOAA-CIRES Climate Diagnostics Center, Boulder, Colorado, USA, from their Web site at http://www.cdc.noaa.gov/

The series selected for this work are monthly averages and long-term mean for surface Pressure; surface, 500, and 300 mb Temperature; surface Precipitable Water Vapour; and 850, 500, and 300 mb Specific Humidity. The series start from January 1948 to September 2000, for a grid point located at 25.0º S latitude, 70.0º W longitude.

## 2.5.- Reliability of the atmospheric reanalysis

The NCEP/NCAR reanalysis produce a 52-year daily atmospheric and surface fields, which, for some variables, is close to a best estimate of the evolving state of the atmosphere. The analysis cycle, with the use of the 6-hour forecast as a first guess, is able to transport information from data-rich to data-poor regions, so that even in relatively data-void areas the reanalysis can estimate the evolution of the atmosphere over both synoptic and climatological timescales.

According to [1], upper-air mass, temperature fields, *u-v* winds, (A-class) are generally well defined by the observations and, given the statistical interpolation of observations and first guess, provide an estimate of the state of the atmosphere better than would be obtained using observations alone. Pressure and temperatures at ground level, relative humidity, precipitable water vapour, (B-class) are partially defined by the observations but are also strongly influenced by the model characteristics.

Thousands of studies have used NCEP/NCAR Reanalysis data over the years. Recently, it has been noted that although the reanalysis system has remain essentially unchanged during the 50 years processed, there were two major changes in the observing system [14]. The first took place during 1948-1957, when the upper-air network was gradually being established, and the second in 1979 when the global operation use of satellite soundings was introduced. This new satellite data resulted in a significant change in the climatology, especially above 200 mb and south of 50º S, suggesting that the climatology based on 1979 to present day is more reliable. The 8-day "reforecasts" indicate that the first decade is much less reliable than the last four.

The same authors indicate that reanalysis can be used for daily to seasonal and interannual timescales. Because of the changes in the observing system, estimation of trends (interdecadal) with the reanalysis is not recommended. However, if it is attempted, several checks should be also performed. Among them:

a) Check the observational coverage that was available to the reanalysis, and remember that rawinsonde observations are much more important than surface observations for reanalysis (remember that the rawinsonde observing networks for Antarctica and the West Coast of South America did not start until July 1957).

b) Compute the trends for the periods before and after 1979 separately. The climatology before 1979 is more dominated by the model climatology in data sparse areas, leading to the generation of spurious trends.

c) Compute the trends for more than one reanalysis. Agreement among the reanalyses increases their reliability, although it is not sufficient to ensure it.

### 2.5.1.- The Visviri experiment

An important work to compare the NCEP/NCAR reanalysis data with upper-air observations in the South American Altiplano is presented in [15]. This is part of a project aimed to improve the understanding of regional climate dynamics during the wet season in the South American Altiplano. Intensive surface and upper-air measurements (4 rawinsonde measurements per day) were carried out at Visviri (17.60° S, 69.50° W, 4,070 m) during two 10-days periods in January 1994 (Visviri I) and January 1995 (Visviri II). Soundings were performed at 09:00, 13:00, 17:00 and 21:00 hours (local time) in Visviri I, and at 09:00, 13:00, 18:00 and 24:00 hour (local time) during Visviri II. The average vertical profiles of temperature, humidity, wind and geopotential height, and the associated diurnal cycles were compared with those obtained from the NCEP/NCAR reanalysis at the closest grid point (17.50° S, 70.00° W).

The result of this comparison shows that reanalysis captures the major features in the vertical structure of these variables and also the interannual changes from a relatively wet period in Visviri I to a much drier conditions in Visviri II. Nevertheless, some discrepancies, both in the strength and timing of the diurnal cycle and particularly in the westward transport of water vapour across the Andes, were found. These values are significantly underestimated by the reanalysis. There are also significative differences at ground level.

These surface and daily cycle differences have been considered at the Department of Geophysics of University of Chile. Apparently, different reanalysis vertical level data than the used in Aceituno and Montecinos [15] can reduce these discrepancies (R. Garreaud 2000, personal communication).

The results obtained in [15] are coherent with the final comments of [14] on that the NCEP/NCAR reanalysis data has proved to be particularly useful in the study of the spatial pattern of climate variability at different timescales. Daily, seasonal, and interannual variability is well captured by reanalysis, though long-term trends are not well represented specially in the southern hemisphere because of the sparse data and that the observation network started at a much later time that in most of the northern hemisphere.

### 2.5.2.- Comparison for the Chajnantor Area

Another important work that compares NCEP/NCAR Reanalysis data with ground observations is presented in the work of Bustos et al [16]. This work compared NCEP/NCAR data on a grid point located 60 Km north from Chajnantor in north-western Chile (II Region) with Chajnantor ground stations data for a 5-year period. The comparison of the NCEP/NCAR reanalysis data and the actual data measured on site during the last five years is very good and thus it is believed that the reanalysis data can be used to study the long-term climatological variations on Chajnantor. Cross-correlation values obtained for monthly average series of PWV and Temperature are 0.79 and 0.87 respectively.

For the PWV comparison, the work showed that the PWV data determined from a 225 GHz opacity measurements is well followed by reanalysis. Tendencies for the PWV during summers from 1996 to 2000 were found similar, and the signature of the winters was clearly seen. However, during part of the time the reanalysis PWV data did not agree on magnitude with measured PWV radiometer data, specially for the August 1997 to June 1998 period.

For the temperature comparison, NCEP/NCAR reanalysis temperature data followed the same trend as the temperature observed at Chajnantor. In fact, a cross-correlation value of 0.87 indicated a good reliability of the reanalysis temperature data. Maximum temperatures during summer of 1998 and 1999 was underestimated by reanalysis, though descending tendencies of average temperatures during summer of 1998 to 2000 were captured in both cases.

# 3.- Climatology of Atacama and some estimations

## 3.1.- Climatology of Atacama

The extremely arid Chilean "Norte Grande" extends north of 30º S, beginning with a lightly humid area where the marine layer can penetrate far inland along a few deep transversal valleys. Beyond the Copiapo River at 27º S, the arid Atacama Desert extends along the central depression or pampas between the Andes and the coastal range, with minor interruptions up to the Peruvian border. Chile raises from the Pacific Ocean along a fault cliff which explains the narrowness of coastal plains and the continental shelf. The extraordinary persistence and intensity of the subtropical anticyclone has been attributed to the presence of the Andes Cordillera that prevents an eastward drift of the system and the stabilising effect of the Humboldt Current [17].

From west to east, three distinct arid zones can be identified through the Chilean Desert. The westernmost portion corresponds to the coastal desert, generically used for those arid areas under the permanent influence of the marine layer. Typical elevations of 1,500 [m] restrict the inland influence of the moist marine layer to relatively low areas, where stratocumuli can occasionally penetrate during night-time and early morning hours. It is characterised by small diurnal and annual temperature ranges and with relative humidities between 70 and 80 %. The typical stratocumulus cloud deck defines the vertical boundary of the marine layer almost all the time in winter. However, the clouds get usually thinner or disappear for a few hours in the afternoon. During summertime, clouds do occur about 50 % of the time but they normally dissipate in the late morning. Along the coast, surface pressure has a clear correlation with surface water temperature, with cold temperatures associated to high pressure and vice versa.

The adjacent zone corresponds to the interior or Atacama Desert, extending between the coastal range and the Andean piedmont, western boundary of the area of influence of summer moisture and precipitation. The Atacama is characterised by large diurnal and annual temperature ranges and very low relative humidities in the afternoon. Relative humidities during night-time and morning hours are quite variable, depending on the location and proximity to the coastal mountains. Occasional penetration of dense fogs ("camanchacas") are evidenced by records at Baquedano (23º S) during night-time [19].

The Andean piedmont climate is characterised by having summer precipitation, moderate temperatures throughout the year and gradual increase of rainfall with altitude.

El Niño Southern Oscillation (ENSO) is the most important ocean-atmosphere coupled phenomenon causing global climate variability on interannual time scales. During an "el niño" event, the waters in the Pacific Ocean becomes warmer than usual, while in "La Niña" times, the waters becomes colder in a variable 2 to 6 years period. This change in water temperature triggers a series of global events affecting the local weather conditions, including those at the astronomical observatories [16].

Trends (interdecadal variability) are mostly influenced by a sudden change produced during the mid 70's. An increase in the sea-surface temperature in the Chilean coastal presented in late 1976, increased the air temperature in the complete troposphere. Those changes would be associated with a general intensity weakening of the subsidence inversion (inferred from humidity changes and stratocumuli nubosity) consistent with the decrease of the average value of the Southern Oscillation Index registered as of 1976 [18].

## 3.2.- Ground stations and rawinsonde data near Paranal

The data collection described in section 2.2.1 includes several Chilean ground stations and rawinsonde data. The closest Chilean ground station to the Paranal area is Antofagasta / Cerro Moreno (23.43º S, 70.45º W, 140 m.a.s.l) that obtains rawinsonde data every day at 00:00 and 12:00 UTC and surface observations.

A complete view of ground stations near the Paranal area can be seen on figure 1. The ground stations used for NCEP/NCAR Reanalysis in Peru, Bolivia, Paraguay, Chile, and Argentina that appear on this figure are listed in Appendix 2. Some of these stations are both ground and rawinsonde station. A complete list worldwide can be found at:
http://www.cpc.noaa.gov/products/analysis_monitoring/cdus/prcp_temp_tables/library.txt

The map shows 47 ground stations (green dots). The availability of each station is not always permanent and depends on human factors to send the data correctly to NCAR or to other appropriate organization. Extra data can be obtained from different temporary ground stations or by rawinsonde experiments.

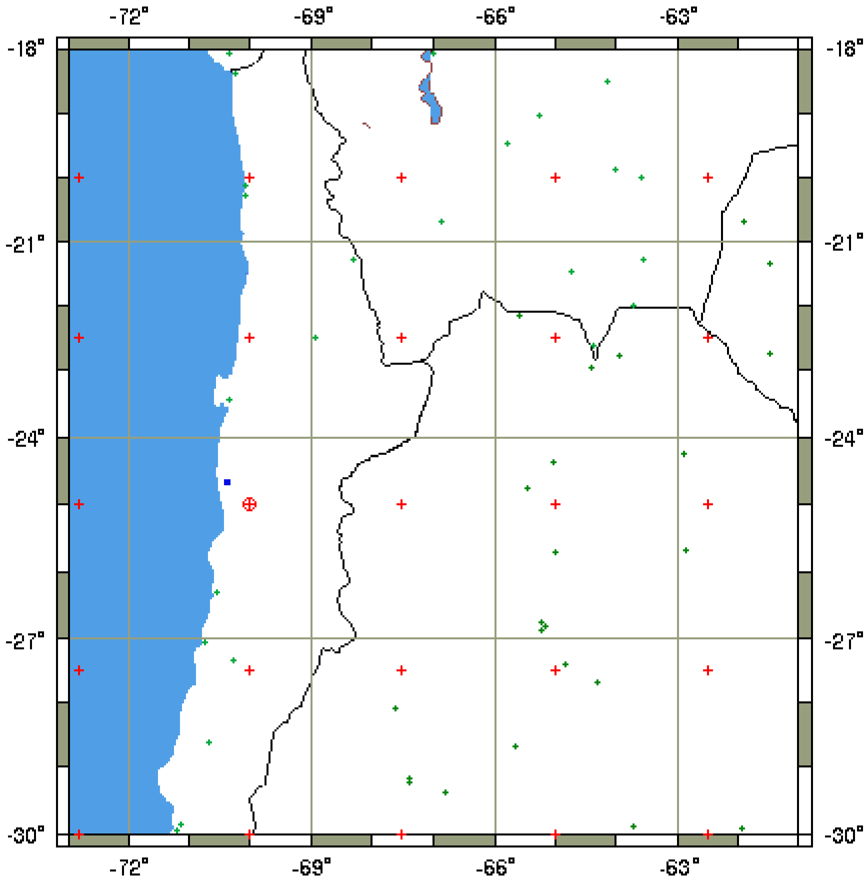


Fig.1: Ground stations are green dotted on the map. Red crosses are gridded points from reanalysis output files. Central red circle corresponds to the closest grid point to the Paranal site (blue square).

## 3.3.- General estimations for Paranal

The main estimation for this work is the use of NCEP/NCAR Reanalysis data at the closest grid point (25.0º S, 70.0º W) to Paranal (24.62º S, 70.40º W). This grid point is located 60 [Km] north-west from Paranal at a geopotential height at the surface of 1,843 [m] according to the NCEP/NCAR reanalysis (D-class variable), but its geographical altitude might be closer to 1,940 [m] according to maps of the area.

As a first estimation, absolute surface values for this grid point do not correspond to absolute values for the Paranal site at 2,635 [m]. However, variations, tendencies, and anomalies of these values can be considered similar at both sites.

# 4.- Methodology

## 4.1.- Downloading the NCEP/NCAR Reanalysis files

The NCEP/NCAR Reanalysis files used for this work are available at: http://www.cdc.noaa.gov/cdc/data.nmc.reanalysis.html

In this web page, there are boxes to select among Pressure Level Data, Surface Data, Surface Flux Data, Other Flux Data, Tropopause Level Data, and T62 Spectral Coefficients. The inputs are the desired variable, pressure level, axis dimension (longitude and latitude), and time range. The selected data are:

| Variable / Selections | Pressure | Temperature | PWV | Specific humidity |
|---|---|---|---|---|
| Type | Monthly average | Monthly average | Monthly average | Monthly average |
| Levels (mb) | Surface | Surface, 500, 300 | Surface | 850, 500, 300 |
| Latitude | 25.0º S | 25.0º S | 25.0º S | 25.0º S |
| Longitude | 70.0º W | 70.0º W | 70.0º W | 70.0º W |
| Begin | Jan. 1948 | Jan. 1948 | Jan. 1948 | Jan. 1948 |
| End | Sept. 2000 | Sept. 2000 | Sept. 2000 | Sept. 2000 |

## 4.2.- GrADS

The Grid Analysis and Display System (GrADS) is an interactive desktop tool that is currently in use world-wide for the analysis and display of earth science data.

GrADS implements a 4-Dimensional data model, where the dimensions are usually latitude, longitude, level, and time. Each data set is located within this 4-Dimensional space by use of a data description file. Both gridded and station data may be described. Gridded data may be non-linearly spaced; Gaussian grids and variable resolution ocean model grids are directly supported. The internal data representation in a file may be either binary, GRIB, or NetCDF (as of version 1.6).

Operations may be performed on the data directly. A rich set of built-in functions is provided. In addition, users may add their own functions as external routines written in any language. The expression syntax allows complex operations that range over very large amounts of data to be performed with simple expressions.

Once the data have been accessed and manipulated, they may be displayed using a variety of graphical output techniques, including line, bar, and scatter plots, as well as contour, shaded contour, streamline, wind vector, grid box, shaded grid box, and station model plots. The user has wide control over all aspects of graphics output, or may choose to use the geophysically intuitive defaults.

The GrADS software used for this work was the UNIX Version 1.7 Beta 9 available at workstations of the Meteorology Section, Department of Geophysics of University of Chile. The GrADS for UNIX workstations current free distribution is in the directory: ftp://grads.iges.org/grads/1.7.beta9

The data obtained from NCEP/NCAR Reanalysis is in NetCDF format (.nc extension). This file is read with GrADS software and then saved in binary format (.bin extension). This step is done in order to manipulate the data in Matlab.

### 4.3.- Matlab

MATLAB is a well-known integrated technical computing environment that combines numeric computation, advanced graphics and visualization, and a high-level programming language.

In this work, the data is obtained from GrADS in binary format. The files contain 1 monthly average data per variable (624 months in 52 years and 9 months in the year 2000). The data is then organized on a 12 x 53 matrix (original matrix), starting from 1 (January) to 12 (December) and from 1 (1948) to 53 (2000). This is performed for every variable at every pressure level. The last 3 months of 2000 are considered as NaN (Not a Number).

Long-term mean vector (1x12) consists in the total monthly average throughout the 53 years, starting from 1 (January) to 12 (December).

Anomalies matrix (12 x 53) are obtained extracting the original matrix with the long-term mean vector for each year. Anomalies are computed for temperature, specific humidity, and precipitable water vapour.

# 5.- Data Analysis

The analyses of the data are observed on figures 2, 3, 4, and 5. Anomalies are studied from 1954 and on because a very strong signal appears for the years 1949-1953, especially for the PWV variable. This signal is probably an overestimation from reanalysis of this variable (pressure, specific humidity, and temperature as well) due to very poor observational data at that time. Anomalies are computed subtracting a long-term mean to the original matrix from 1954 to the present, avoiding the strong 1949-1953 signal.

Coloured isopleth diagrams (annually versus monthly values) for the period 1948-2000 (from 1954 for anomalies) are shown. Figure 2 shows pressure and temperature at the surface and its anomalies. Figure 3 shows precipitable water vapour and anomalies. It also plots values and anomalies for January, February and October. Anomalies of PWV expressed in percentages are depicted on figure 4. Figure 5 shows the values for temperature (500 and 300 mb) and specific humidity (850, 500, and 300 mb) and its anomalies.

## 5.1.- Pressure

Pressure level and anomalies at the surface are obtained for the period from 1948-2000. Figure 2 shows a year cycle with higher pressures during winter. Positive anomalies can be seen starting in the mid 70's. This change has also been noted in [18].

## 5.2.- Temperature

Temperature and anomalies on surface are on figure 2, showing a strong negative anomaly for the last 2 years, comparable with the observed in 1955. It is also noted in the anomalies plot an increase of temperature in the mid 70's until 1998. At higher levels, for 500 and 300 mb on figure 5, the strong negative anomalies for the last 2 years are weakened.

## 5.3.- Precipitable water vapour

PWV, anomalies, and a time series for January, February and October are shown on figure 3. PWV has a remarkable annual cycle, with low values during austral winter and higher values from December to March. A strong signal appears in 1949-53, apparently an overestimation of reanalysis due to poor observational data. It can be seen that anomalies during January to March alternates throughout the years. The lowest values of PWV are observed during October. Anomalies in percentage are on figure 4, showing anomalies less than ± 50 % throughout the years.

## 5.4.- Specific humidity

Specific humidity is analysed at 850, 500, and 300 mb levels. It has similar results than for PWV. At 850, 500 and 300 mb, figure 5 shows a very dry atmosphere during most of the year. High signals of water vapour in the atmosphere appear for the January-March period at 850 mb, while at 300 mb, high signals appear for the March-June period for the last 30 years.

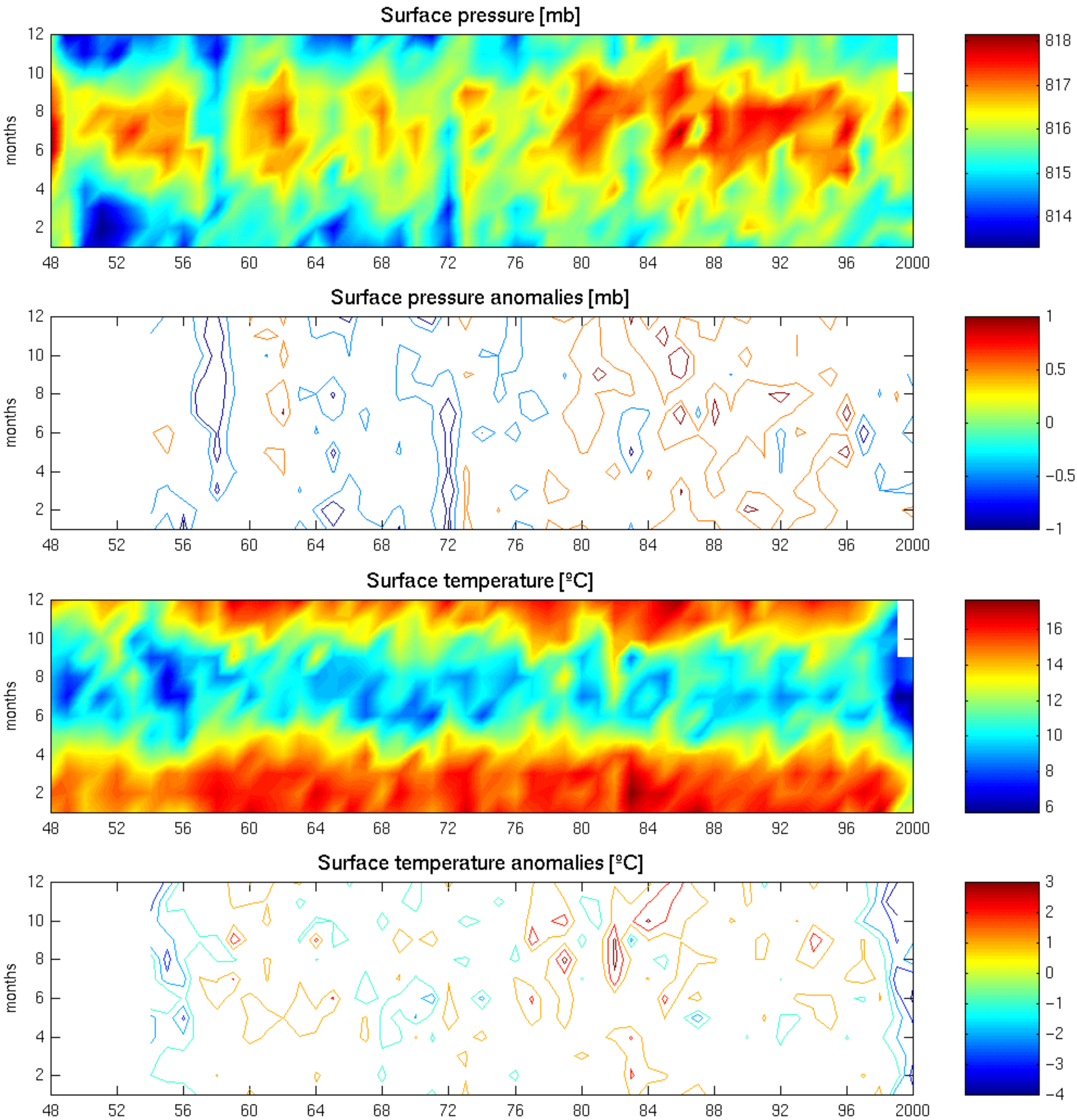
Surface pressure [mb]
months
818
817
816
815
814
Surface pressure anomalies [mb]
1
0.5
0
−0.5
−1
Surface temperature [ºC]
16
14
12
10
8
6
Surface temperature anomalies [ºC]
3
2
1
0
−1
−2
−3
−4
48
52
56
60
64
68
72
76
80
84
88
92
96
2000

Figure 2

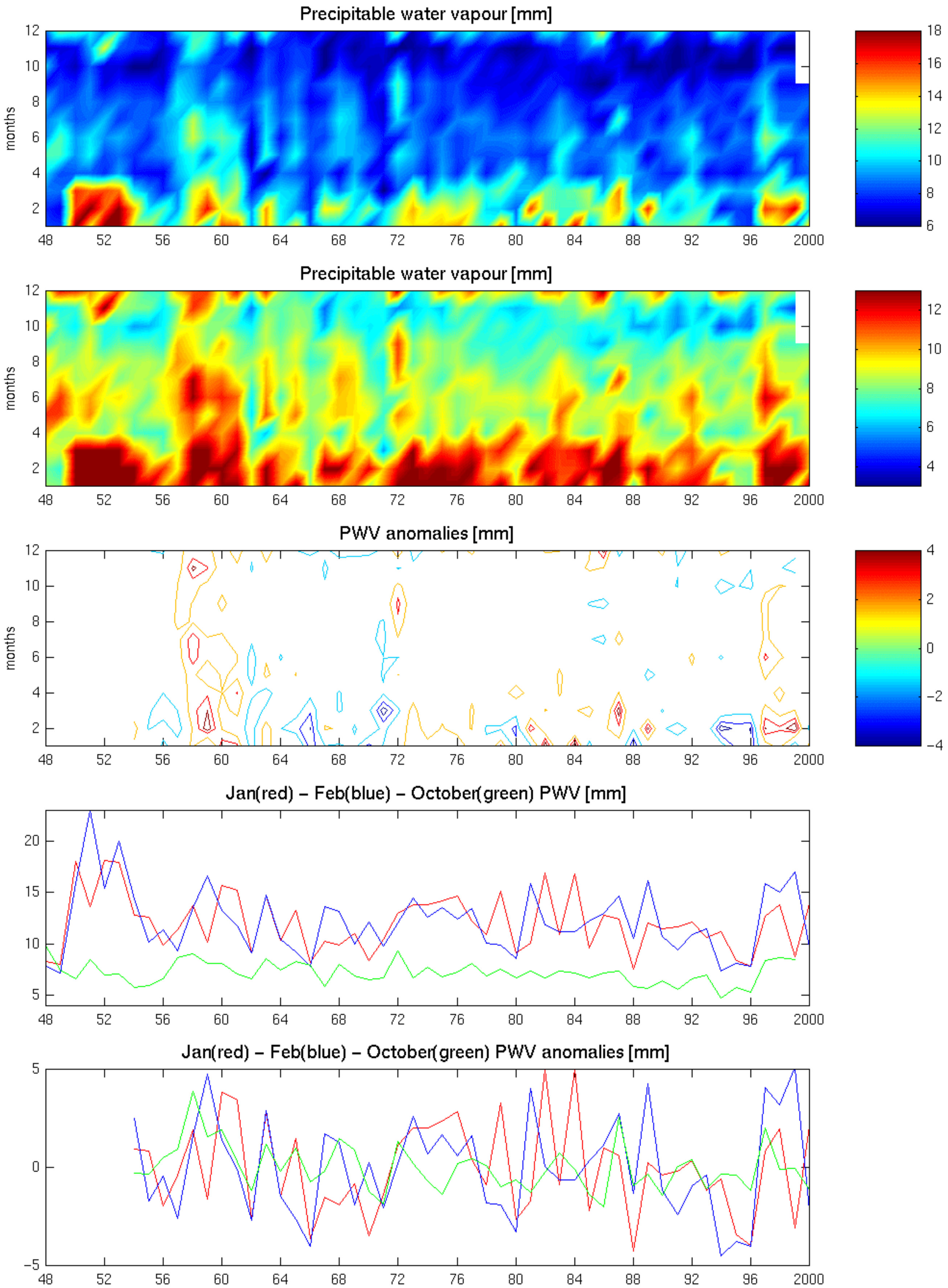

Precipitable water vapour [mm]
months
Precipitable water vapour [mm]
months
PWV anomalies [mm]
months
Jan(red) – Feb(blue) – October(green) PWV [mm]
Jan(red) – Feb(blue) – October(green) PWV anomalies [mm]


Figure 3

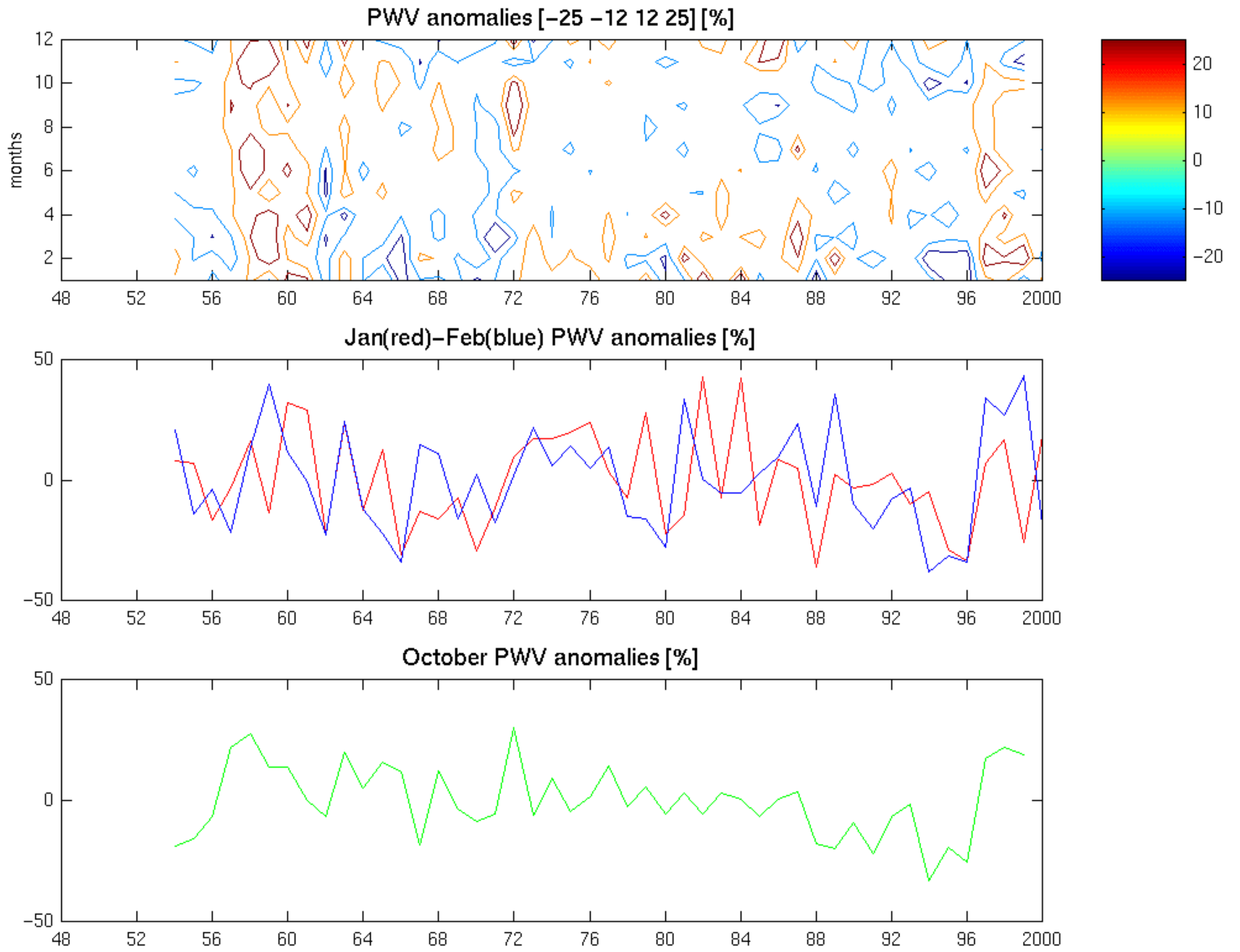
PWV anomalies [−25 −12 12 25] [%]
months
Jan(red)−Feb(blue) PWV anomalies [%]
October PWV anomalies [%]

Figure 4

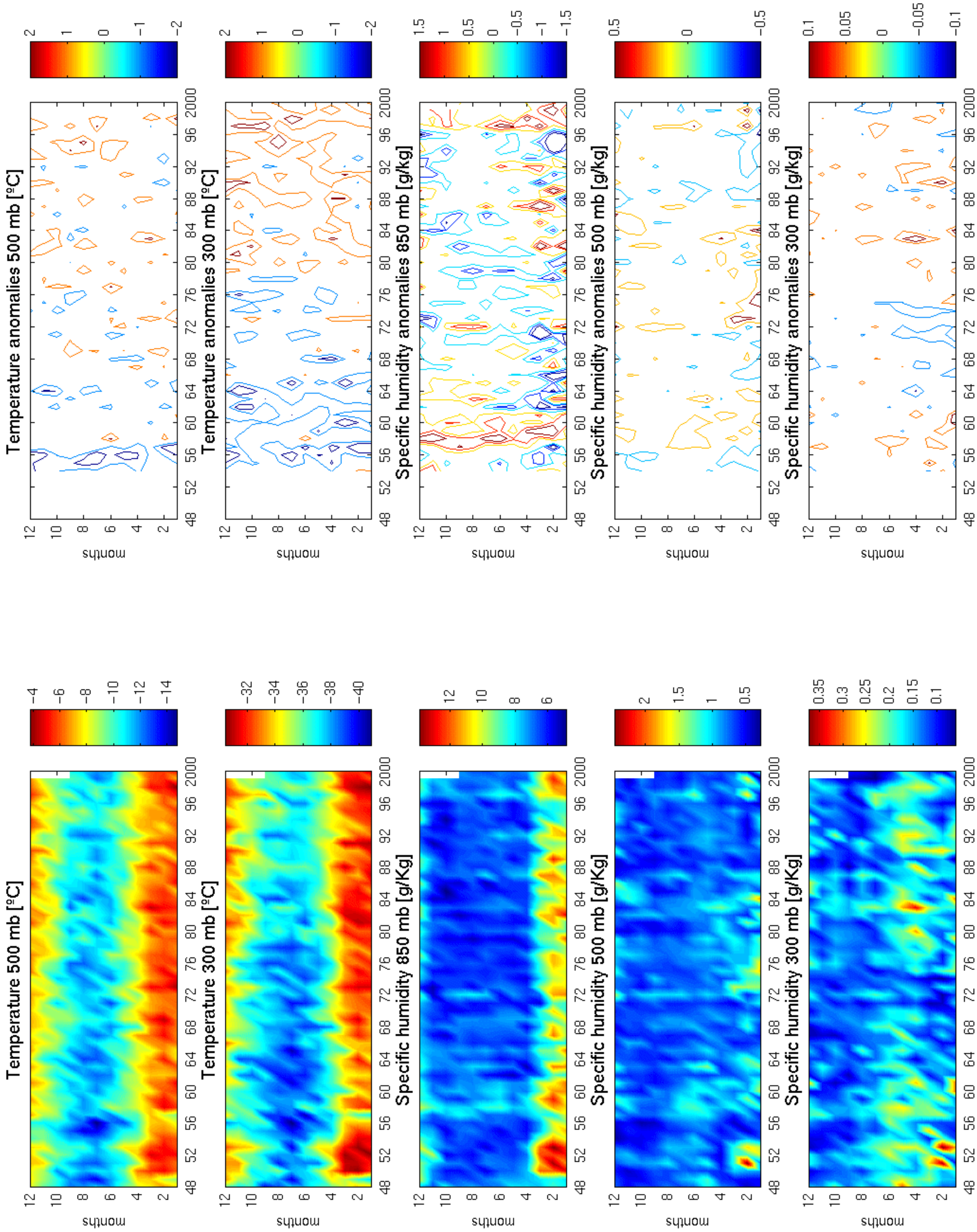
Temperature 500 mb [ºC]
Temperature 300 mb [ºC]
Specific humidity 850 mb [g/Kg]
Specific humidity 500 mb [g/Kg]
Specific humidity 300 mb [g/Kg]
Temperature anomalies 500 mb [ºC]
Temperature anomalies 300 mb [ºC]
Specific humidity anomalies 850 mb [g/kg]
Specific humidity anomalies 500 mb [g/kg]
Specific humidity anomalies 300 mb [g/kg]
months

Figure 5

# 6.- Conclusions and future work

From the relevant figures, an annual cycle for the PWV is well defined with a dry winter and wetter summers. During austral winter (May-October), the PWV has a stable and relatively low values throughout the years. During summer (January-March) this situation changes and a higher amount of water vapour is present in the atmosphere with a variable 1-5 year cycle.

During austral summer, the PWV monthly averages show values between 7 and 17 mm and the anomalies do not exceed more than ± 5 mm throughout the years (except for the 1949-1953 period, considered an overestimation of the reanalysis due to poor observational data). It is reminded here that these values are for a site of 1,843 m.a.s.l and can be corrected for Paranal (792 m altitude difference) with the same altitude correction method used in [16]. Performing an FFT (Fast Fourier Transform) to the PWV summer time series (January-March), a variable 1-5 year cycle (coincident with ENSO spacing) and longer period cycles of 7 and 11.5 years are found.

It is noted that positive PWV anomalies have occurred during the summers of years 1997 to 2000, being these years wetter periods than usual. Nevertheless, these wet summers periods are normal in a 52-year historical context and, probably, the cycle should lead to a drier period. It is also noted that the previous cycle (summer periods of years 1993 to 1996) are dominated by negative anomalies.

The surface air temperature anomalies (Fig. 3) shows a cooler air temperature until 1976 and changes to a warmer air temperature after 1976, corroborating the results of Rutllant et al [18]. No evidences are found to consider the recommendation of Kistler et al [14] to analyse the periods before and after 1979 separately due to the introduction of new satellite data. From the results, it is not possible to see a change on the data that can be attributed to the different observations used, and the change in temperature in 1976 is produced by an interdecadal variability [18]. For the last two years, a strong negative surface temperature anomaly is observed in contrast with positive anomalies for air temperature at 500 and 300 mb.

The variable 1-5 year PWV anomaly cycle can be analysed in the future, probably having an ENSO connection.

Previous works comparing the results of measured data with NCEP/NCAR Reanalysis [14] [15] [16], have proved that daily, seasonal and interannual variability is well captured by reanalyses, though trends are not well captured specially before 1979 for the Southern Hemisphere. The fact that the closest grid point to Paranal is at a different height and at a ~60 km distance plus the introduction of new observing systems over the years, makes it necessary to perform a cross-correlation analysis between the NCEP/NCAR Reanalysis data and historical meteorological data obtained in Paranal in order to guarantee the value of NCEP/NCAR Reanalysis as a good indicator of the climatology over the Paranal area.

A very important parameter to be determined for the Paranal area is the monitoring of cloudiness. Scanning radiometers onboard NOAA polar-orbiting satellites measure the earth's total longwave emmitance OLR (Outgoing Longwave Radiation) and these data is available from 1974 to the present. The radiometers sense energy in a visible and infrared window region from which albedo and longwave flux is determined. The estimation of total OLR flux is done by using a regression model derived from radiation calculations made for 99 different atmospheres covering a broad range of temperatures and moisture as well as overcast and clear sky conditions with a superior fit of 98% of the total variance [20]. Thus, the OLR data have been used in a variety of diagnostics and climate sensitivity studies and have been particularly useful for monitoring cloudiness and rainfall over the tropics. More recently, the ENSO events have been revealed in great detail by the OLR data [21].


# Acknowledgments

Special thanks are given to Dr. José Rutllant for the access to documentation and for the authorisation to use the facilities at the Meteorology Section of the Department of Geophysics, University of Chile. I also thank Dr. Guillermo Delgado (Onsala Space Observatory / European Southern Observatory) for the review of this manuscript.


# 7.- References


[1] Kalnay, E. et al., 1996: "The NCEP/NCAR 40-Year Reanalysis Project", *Bulletin American Meteorological Society,* **77**, 437-471.

[2] Matthews, E., 1985: Atlas of archived vegetation, land-use and seasonal albedo data sets. NASA Tech. Memo. 86199, 53 pp. [Available from Goddard Space Flight Center, Greenbelt, MD 20771]

[3] Pan, H.-L., and Mahrt, L., 1987: "Interaction between soil hydrology and boundary-layer development". *Bound.-Layer Meteor.*, **38**,185-220.

[4] Mahrt, L., and Pan, H.-L., 1984: "A two-layer model of soil hydrology". *Bound.-Layer Meteor.*, **29**, 1-20.

[5] Dorman, J. L., and Sellers, P. J., 1989: "A global climatology of albedo, roughness length and stomatal resistance for atmospheric general circulation models as presented by the Simple Biosphere Model (SB)". *J. Appl. Meteor.*, **28**, 833-855.

[6] Parrish, D. F., and Derber, J. C., 1992: "The National Meteorological Center's spectral statistical interpolation analysis system". *Mon. Wea. Rev.*, **120**, 1747-1763.

[7] Derber, J. D., Parrish, D. F., and Lord, S. J., 1991: "The new global operational analysis system at the National Meteorological Center". *Wea. Forecasting*, **6**, 538-547.

[8] Kanamitsu, M., 1989: "Description of the NMC global data assimilation and forecast system". *Wea. Forecasting*, **4**, 334-342.

[9] Kanamitsu, M., et al., 1991: "Recent changes implemented into the global forecast system at NMC". *Wea. Forecasting*, **6**, 425-435.

[10] Gandin, L. S., 1988: "Complex quality control of meteorological observations". *Mon. Wea. Rev.*, **116**, 1138-1156.

[11] Woollen, J. S., 1991: "New NMC operational OI quality control". Preprints, *Ninth Conf. on Numerical Weather Prediction*, Denver, CO, Amer. Meteor. Soc., 24-27.

[12] Woollen, J. S., et al., 1994: "Quality control in the reanalysis system". Preprints, *10th Conf. on Numerical Weather Prediction*, Portland, OR, Amer. Meteor. Soc., 13-14.

[13] Gandin, L. S., 1993: "Optimal averaging of meteorological fields". NMC Office Note 397, 45 pp. [Available from NOAA/NCEP, 5200 Auth. Rd. Washington, DC, 20233.]

[14] Kistler, R., Kalnay, E., et al. "The NCEP/NCAR 50-Year Reanalysis". Submitted to the *Bulletin American Meteorological Society,* June 16, 2000.

[15] Aceituno, P., Montecinos, A., 2000: "Diurnal cycle over the South American altiplano: comparison of NCEP/NCAR reanalysis with upper-air observations during the Visviri field experiment". *Sixth International Conference on Southern Hemisphere Meteorology and Oceanography*, P4.28.

[16] Bustos, R., Delgado, G., Nyman, L., and Radford, S., 2000: "52 years of climatological data for the Chajnantor area" ALMA Memo Series No. 333.

[17] Rutllant, J., 1977: "On the extreme aridity of coastal and atacama deserts in northern Chile". Thesis submitted for the degree of Ph. D. (Meteorology) at the University of Wisconsin-Madison.

[18] Rutllant, J., Fuenzalida, H., Torres, R., and Figueroa, D., 1998: "Interacción océano-atmósfera-tierra en la Región de Antofagasta (Chile, 23ºS): Experimento DICLIMA". *Revista Chilena de Historia Natural*, **71**, 405-427.

[19] Rutllant, J., Ulriksen, P., Sippa, J., Salinas, H., and Doerr, L., 1972: "Resultados de la campaña de mediciones meteorológicas realizada en la provincia de Antofagasta". Publ. Nº 140 Department of Geophysics, University of Chile. Santiago, Chile.

[20] Gruber, A., and A. F. Krueger, 1984: "The status of the NOAA outgoing longwave radiation data set". *Bull. Amer. Meteor. Soc.*, **65**, 958-962.

[21] Liebmann, B., and C. A. Smith, 1996: "Description of a complete (interpolated) outgoing longwave radiation dataset". *Bull. Amer. Meteor. Soc.*, **77**, 1275-1277.

# Appendix 1

The output variables are classified into four categories. A indicates that the analysis variable is strongly influenced by observed data (e.g., upper-air temperature and wind). B indicates that, although there are observational data, the model also has a very strong influence on the analysis value (e.g., humidity and surface temperature). C indicates that there are no observations directly affecting the variable, so that it is derived solely from the model fields forced by the data assimilation to remain close to the atmosphere (e.g., clouds and precipitation). Finally, D represents a field that is fixed from climatological values and does not depend on the model (e.g., plant resistance, land-sea mask). The standard GRIB output variables are presented.

*a. Standard GRIB output*

Pressure coordinate output in a regular (2.5º lat x 2.5º long) grid. All fields are instantaneous values at a given time:

| Class | Field Type |
|---|---|
| A | Geopotential height (gpm) at 17 levels |
| A | *u* wind (m $s^{-1}$) at 17 levels |
| A | *v* wind (m $s^{-1}$) at 17 levels |
| A | Temperature (K) at 17 levels |
| B | Pressure vertical velocity (Pa $s^{-1}$) at 12 levels |
| B | Relative humidity (%) at 8 levels |
| A | Absolute vorticity ($s^{-1}$) at 17 levels |
| A | *u* wind of the lowest 30-mb layer (m $s^{-1}$) |
| A | *v* wind of the lowest 30-mb layer (m $s^{-1}$) |
| B | Temperature of the lowest 30-mb layer (K) |
| B | Relative humidity of the lowest 30 mb (%) |
| B | Pressure at the surface (Pa) |
| B | Precipitable water vapour (kg $m^{-2}$) |
| B | Relative humidity of the total atmospheric column (%) |
| A | Temperature at the tropopause (K) |
| A | Pressure at the tropopause (Pa) |
| A | *u* wind at the tropopause (m $s^{-1}$) |
| A | *v* wind at the tropopause (m $s^{-1}$) |
| A | Vertical speed shear at the tropopause (1 $s^{-1}$) |
| B | Surface lifted index (K) |
| B | "Best" (4 layer) lifted index (K) |
| A | Temperature at the maximum wind level (K) |
| A | Pressure at the maximum wind level (Pa) |
| A | *u* wind at the maximum wind level (m $s^{-1}$) |
| A | *v* wind at the maximum wind level (m $s^{-1}$) |
| D | Geopotential height at the surface (gpm) |
| A | Pressure reduced to MSL (Pa) |
| B | Relative humidity in three sigma layers: 0.44-0.72, 0.72-0.94, 0.44-1.0 (%) |
| B | Potential temperature at the lowest sigma level (K) |
| B | Temperature at the lowest sigma level (K) |
| B | Pressure vertical velocity at the lowest sigma level (Pa $s^{-1}$) |
| B | Relative humidity at the lowest sigma level (%) |
| B | *u* wind at the lowest sigma level (m $s^{-1}$) |
| B | *v* wind at the lowest sigma level (m $s^{-1}$) |

*b.* *Output levels*

Standard pressure levels (mb):

| | | | | | | | | |
|---|---|---|---|---|---|---|---|---|
| 1000 | 925 | 850 | 700 | 600 | 500 | 400 | 300 | 250 |
| 100 | 150 | 100 | 70 | 50 | 30 | 20 | 10 | |

# Appendix 2

Here is the list of meteorological stations for Peru, Bolivia, Paraguay, Chile, and Argentina that appear as green dots on Figure 1. A complete list of ground stations around the world is available at
http://www.cpc.noaa.gov/products/analysis_monitoring/cdus/prcp_temp_tables/library.txt

Legend:

| | |
|---|---|
| Stnid | - 5 character WMO station identifier |
| Lat | - latitude in hundredths, ex: 7093 = 70.93 n ; -1093 = 10.93 s |
| Lon | - longitude in hundredths, ex: 34637 = 346.37 if lon > 180 lon = 360 - lon |
| Elev | - station elevation in whole meters |
| Call | - station identification call letters if available |

| Stnid | Lat | Long | Elev | Call | | | City | Country |
|---|---|---|---|---|---|---|---|---|
| 84782 | -1807 | 7030 | 458 | 192 | 99 | 0sptn | Tacna/Ciriani | Peru |
| 85242 | -1805 | 6707 | 3702 | 194 | 99 | 0slor | Oruro/Juan_Mendoza | Bolivia |
| 85264 | -1850 | 6410 | -999 | 194 | 99 | 0 | Vallegrande | Bolivia |
| 85283 | -1902 | 6527 | 2903 | 194 | 99 | 0slsu | Sucre/Juana_Azurduy | Bolivia |
| 85293 | -1953 | 6572 | 3934 | 194 | 99 | 0slpo | Potosi/Rojas | Bolivia |
| 85312 | -1983 | 6400 | -999 | 194 | 99 | 0 | Monteagudd | Bolivia |
| 85315 | -2005 | 6357 | 792 | 194 | 99 | 0slca | Camiri | Bolivia |
| 85322 | -2058 | 6680 | 3670 | 194 | 99 | 0 | Uyuni | Bolivia |
| 85345 | -2127 | 6350 | 400 | 194 | 99 | 0slvm | Villa_Montes/Rafael | Bolivia |
| 85364 | -2153 | 6472 | 1858 | 194 | 99 | 0sltj | Tarija/Capt_Oriel | Bolivia |
| 85365 | -2202 | 6370 | 617 | 194 | 99 | 0slya | Yacuiba | Bolivia |
| 85394 | -2275 | 6338 | -999 | 194 | 99 | 0 | Bermejo | Bolivia |
| 86017 | -2072 | 6192 | 315 | 196 | 99 | 0 | Fortin Nueva Asuncion | Paraguay |
| 86038 | -2133 | 6150 | 190 | 196 | 99 | 0 | La Patria | Paraguay |
| 86065 | -2270 | 6150 | 220 | 196 | 99 | 0 | Prats-Gil | Paraguay |
| 85406 | -1835 | 7033 | 55 | 195 | 99 | 0scar | Arica/Chacalluta | Chile |
| 85417 | -2022 | 7015 | 5 | 194 | 98 | 1 | Iquique/Cavancha | Chile |
| 85418 | -2053 | 7018 | 48 | 195 | 99 | 0scda | Iquique/Diego_Arac | Chile |
| 85424 | -2122 | 6827 | 3695 | 195 | 99 | 1 | Oyahue | Chile |
| 85432 | -2250 | 6890 | 2320 | 195 | 99 | 1sccf | Calama/El_Loa | Chile |
| 85442 | -2343 | 7045 | 140 | 195 | 99 | 0scfa | Antofagasta/Cerro | Chile |
| 85460 | -2632 | 7062 | 30 | 195 | 99 | 0scra | Chanaral | Chile |
| 85466 | -2707 | 7080 | 55 | 195 | 99 | 0 | Caldera | Chile |
| 85470 | -2730 | 7042 | 290 | 195 | 99 | 0scha | Copiapo/Chamonate | Chile |
| 85486 | -2860 | 7077 | 526 | 195 | 99 | 0scll | Vallenar | Chile |
| 85488 | -2992 | 7120 | 146 | 195 | 99 | 0scse | La_Serena/LaFlorida | Chile |
| 85500 | -2995 | 7137 | 25 | 195 | 99 | 1 | Coquimbo | Chile |
| 87007 | -2210 | 6560 | 3462 | 199 | 99 | 0sasq | La_Quiaca_Observat | Argentina |
| 87016 | -2315 | 6432 | 357 | 199 | 99 | 0saso | Oran_Airport | Argentina |
| 87022 | -2265 | 6382 | 450 | 199 | 99 | 0sast | Tartagal_Airport | Argentina |
| 87046 | -2438 | 6508 | 1167 | 199 | 99 | 0sasj | Jujuy_Airport | Argentina |
| 87047 | -2485 | 6548 | 1216 | 199 | 99 | 0sasa | Salta_Airport | Argentina |
| 87052 | -2578 | 6498 | 779 | 198 | 98 | 0 | Rosario De La Fro | Argentina |

| | | | | | | | | | |
|---|---|---|---|---|---|---|---|---|---|
| 87065 | -2417 | 6290 | 205 | 199 | 99 | 0 | sasr | Rivadavia | Argentina |
| 87071 | -2575 | 6287 | 220 | 199 | 99 | 0 | | Monte Quemado | Argentina |
| 87116 | -2680 | 6520 | 481 | 198 | 98 | 1 | | Tucuman Observatory | Argentina |
| 87120 | -2683 | 6520 | 421 | 198 | 98 | 0 | | Tucuman | Argentina |
| 87121 | -2685 | 6510 | 450 | 199 | 99 | 0 | sant | Tucuman/Teniente | Argentina |
| 87127 | -2745 | 6488 | 281 | 198 | 98 | 0 | | Rio Hondo | Argentina |
| 87129 | -2777 | 6430 | 199 | 199 | 99 | 0 | sane | Santiago_Del_Estero | Argentina |
| 87211 | -2807 | 6757 | 1201 | 199 | 99 | 0 | sani | Tinogasta | Argentina |
| 87213 | -2923 | 6743 | 945 | 199 | 99 | 0 | | Anguinan_Airport | Argentina |
| 87214 | -2922 | 6743 | 950 | 199 | 99 | 0 | sano | Chilecito | Argentina |
| 87217 | -2938 | 6682 | 429 | 199 | 99 | 0 | sanl | La_Rioja/Capt_Vicen | Argentina |
| 87222 | -2860 | 6577 | 454 | 199 | 99 | 0 | sanc | Catamarca_Airport | Argentina |
| 87244 | -2990 | 6368 | 341 | 199 | 99 | 0 | sacv | Villa_Maria_Del_Rio | Argentina |
| 87257 | -2988 | 6195 | 88 | 199 | 99 | 0 | sanw | Ceres | Argentina |

# A 52-Year Climatological Study
# For the Paranal Area
# Using NCEP/NCAR Reanalysis Data

Ricardo Bustos Placencia
Civil Electrical Engineer
University of Chile
Email: rbustos@dgf.uchile.cl

Presented to the European Southern Observatory
Paranal Observatory

November 2000

# Index